

Densities and temperatures in the Venus mesosphere and lower thermosphere retrieved from SOIR on board Venus Express: Carbon dioxide measurements at the Venus terminator

A. Mahieux,¹ A. C. Vandaele,¹ S. Robert,¹ V. Wilquet,¹ R. Drummond,¹ F. Montmessin,^{2,3} and J. L. Bertaux^{2,3}

Received 2 February 2012; revised 19 April 2012; accepted 18 May 2012; published 3 July 2012.

[1] SOIR is a high-resolution spectrometer flying on board the ESA Venus Express mission. It performs solar occultations of the Venus high atmosphere, and so defines unique vertical profiles of many of the Venus key species. In this paper, we focus on the Venus main constituent, carbon dioxide. We explain how the temperature, the total density, and the total pressure are derived from the observed CO₂ density vertical profiles. A striking permanent temperature minimum at 125 km is observed. The data set is processed in order to obtain a Venus Atmosphere from SOIR measurements at the Terminator (VAST) compilation for different latitude regions and extending from 70 up to 170 km in altitude. The results are compared to many literature results obtained from ground-based observations, previous missions, and the Venus Express mission. The homopause altitude is also determined.

Citation: Mahieux, A., A. C. Vandaele, S. Robert, V. Wilquet, R. Drummond, F. Montmessin, and J. L. Bertaux (2012), Densities and temperatures in the Venus mesosphere and lower thermosphere retrieved from SOIR on board Venus Express: Carbon dioxide measurements at the Venus terminator, *J. Geophys. Res.*, *117*, E07001, doi:10.1029/2012JE004058.

1. Introduction

[2] The Venus terminator in the mesosphere and thermosphere is a region of great interest as a transition between the hot dayside and the cold nightside of the Venus atmosphere [Keating *et al.*, 1980]. It was previously supposed that a compression of the atmosphere at these locations might induce large temperature variations, due to the same pressure levels altitude difference between the dayside and the nightside of the planet (C. Parkinson, private communication, 2012). However, these are poorly known, since only a few measurements were obtained at these particular local solar times, i.e., 6:00 A.M. and 6:00 P.M. The SOIR instrument on board Venus Express (VEX) offers the possibility to routinely monitor the density of various key Venus species and temperature vertical profiles [Bertaux *et al.*, 2007b; Fedorova *et al.*, 2008; Vandaele *et al.*, 2008]. SOIR is particularly well suited to help identify the dynamic and chemical processes that take place in this region.

[3] Carbon dioxide is the main component of Venus' atmosphere, with a mean volume mixing ratio (VMR) of 96.5% up to an altitude of 120 km [Keating *et al.*, 1980]. Above this, its VMR decreases with altitude as CO₂ is photodissociated on the dayside of the planet by solar ultraviolet radiation, forming carbon monoxide and excited oxygen atoms. As the main constituent of the Venus atmosphere, carbon dioxide is of great interest in order to describe the physics of the atmosphere at the terminator. The SOIR instrument measures CO₂ absorption across a broad spectral window. The observed atmospheric transmittance spectra are subsequently inverted to obtain vertical density profiles, which extend from 70 km up to 170 km. This paper presents the CO₂ density and temperature profiles of selected orbits that were obtained between 2006 and 2011, and compiles them in order to present a global view of the atmospheric characteristics at the Venusian terminator.

[4] Previously, CO₂ density and temperature have been measured in this particular altitude range and at, or close to, the terminator in the Venus atmosphere from the ground [Clancy *et al.*, 2003, 2008, 2012; Lellouch *et al.*, 1994] (sub-mm range from Earth telescopes) as well as from previous spacecrafts and in situ probes: Pioneer Venus [Fox and Kasprzak, 2007; Keating *et al.*, 1980; von Zahn *et al.*, 1980, and references therein] and VEX instruments [Bertaux *et al.*, 2007b; Irwin *et al.*, 2008; Piccialli *et al.*, 2012; Tellmann *et al.*, 2009]. Models have been developed based on previous measurement data sets obtained during the Pioneer Venus era, such as the VTS3 model of the upper atmosphere [Hedin *et al.*, 1983], the Keating model of the upper atmosphere [Keating *et al.*, 1980] and the Zasova's model

¹Planetary Aeronomy, Belgian Institute for Space Aeronomy, Brussels, Belgium.

²LATMOS, Guyancourt, France.

³Institut Pierre Simon Laplace, Université de Versailles-Saint-Quentin, Guyancourt, France.

Corresponding author: A. Mahieux, Planetary Aeronomy, Belgian Institute for Space Aeronomy, 3 av. Circulaire, B-1180 Brussels, Belgium. (arnaud.mahieux@aeronomie.be)

Published in 2012 by the American Geophysical Union.

from the surface up to 100 km [Zasova *et al.*, 2007, 2006]. Altogether, these measurements and models cover an altitude range between 50 and 200 km, and contain information encompassing the terminator region. Large temporal variations are observed in these data sets.

2. Instrument Description and Observation Geometry

[5] The SOIR instrument has been extensively described in Bertaux *et al.* [2007a], Nevejans *et al.* [2006], and Mahieux *et al.* [2008, 2009, 2010]. We will summarize here only the most important SOIR characteristics.

[6] SOIR is one of the three channels of the SPICAV/SOIR instrument. It is an infrared spectrometer, using an echelle grating as the diffracting element. The accessible wave number range covers the 2200 to 4400 cm⁻¹ region, and is divided into 94 useful diffracting orders, or simply orders, from 101 to 194. The order selection is performed using an acousto-optic tunable filter (AOTF), which allows us much to select and transmit only a small wave number range diffracted by the echelle grating. The resolution of SOIR varies from order to order, with a value of about 0.11 cm⁻¹ in order 101 to 0.21 cm⁻¹ in order 194. The SOIR detector is composed of 320 pixels in its spectral direction. The spectral width of a pixel varies from 0.06 to 0.12 cm⁻¹ and the free spectral range (FSR) has a constant value of 22.4 cm⁻¹. The SOIR useful detector pixels are combined into two groups in the spatial direction called bins. Two simultaneous measurements are thus obtained at two slightly different altitudes corresponding to the 2 bins on the detector. The width of the AOTF bandpass transfer function is ~24 cm⁻¹, while the width of an order varies between 19.3 cm⁻¹ to 37.1 cm⁻¹ with ascending order, which causes an order overlapping on the detector. Moreover, the AOTF transfer function is not zero in the adjacent orders [Mahieux *et al.*, 2009]. To correctly simulate the SOIR measurement, more than one diffraction order have to be taken into account [Mahieux *et al.*, 2010]. Five contiguous diffraction orders are usually simulated, i.e., the scanned one and two adjacent orders on each side.

[7] SOIR performs solar occultation observations of the Venus atmosphere from the VEX spacecraft, which is in a polar orbit with its periapsis located above the North Pole. The vertical size of the instantaneously scanned atmosphere at the limb tangent point varies from a few hundreds of meters for the Northern measurements to tens of kilometers for the Southern measurements. The altitude range probed by SOIR, i.e., where measurements are scientifically meaningful, varies from 70 km up to 170 km. The lower boundary corresponds to total absorption of sunlight by Venus' clouds, and the upper boundary to the detection of the strongest CO₂ band in the selected SOIR wave number range. During an occultation, four different diffraction orders are measured quasi-simultaneously – four sequentially within 1 s, each one lasting 160 ms at maximum. It allows us to study either the same species at different ranges of altitudes, as it will be the case here for CO₂, or different species to obtain volume mixing ratios [Bertaux *et al.*, 2007b; Fedorova *et al.*, 2008; Vandaele *et al.*, 2008]. The occultations are grouped in occultation seasons (OS), which are time periods when the solar occultations take place relative to the VEX spacecraft

orbital configuration. These OS periods occur roughly every three months for one month. The definition of the OS is a parameter linked to the VEX spacecraft orbital characteristics, and has no sense in terms of Venus climatology.

[8] The spectroscopic parameters are obtained from the Hitran 2008 database [Rothman *et al.*, 2009], with corrected values for the pressure broadening coefficients and shifts, to take into account that the atmosphere of Venus is mainly CO₂ instead of nitrogen and oxygen [Vandaele *et al.*, 2008]. Carbon dioxide is studied in the range 2400 to 4000 cm⁻¹ (2.5 to 4.16 μm). In this study we essentially concentrate on the vibrational bands of the following five isotopologues ¹²C¹⁶O₂, ¹³C¹⁶O₂, ¹⁶O¹²C¹⁸O, ¹⁶O¹³C¹⁸O and ¹⁶O¹²C¹⁷O. The isotopic ratio of the carbon and oxygen atoms is assumed to be the same as on Earth [Bézard *et al.*, 1987; Clancy and Muhleman, 1991]. For ¹²C¹⁶O₂, the 20011–10002 and 00021–01101 bands (in Hitran notation [Rothman *et al.*, 2009]) are observed in orders 171 (3822 to 3854 cm⁻¹) and 176 to 180 (3933 to 4057 cm⁻¹), respectively. They give information on low altitudes (70 to 90 km). The 21103–00001 band is measured in order 141 (3151 to 3178 cm⁻¹) and the 21102–00001 band in orders 147 to 150 (3285 to 3381 cm⁻¹); they correspond to mid altitudes (80 to 120 km). Finally the 10012–00001 and 10011–00001 bands are measured in the orders 160 to 168 (3576 to 3787 cm⁻¹) and are observed at very high altitudes from 120 to 170 km. The 10012–00001 band of ¹³C¹⁶O₂ is measured in orders 155 and 156 (3464 to 3516 cm⁻¹); it is measured at high altitude from 100 to 140 km. Three bands of ¹⁶O¹²C¹⁸O are observed, the 01111–00001 band in order 134 (2995 to 3020 cm⁻¹) at low altitude (from 70 to 90 km), and the 20002–00001 and 20003–00001 bands at midaltitude (90 to 120 km) measured in orders 112 (2503 to 2525 cm⁻¹), and 117 and 118 (2615 to 2637 cm⁻¹) respectively. The 20001–00001 band of the ¹⁶O¹³C¹⁸O isotopologue is observed in order 121 (2704 to 2727 cm⁻¹) at low altitude, from 70 to 90 km.

3. Retrieval Method Description

[9] The core of the algorithm used in this paper, Asimat, has been described previously in the companion paper [Mahieux *et al.*, 2010]. However, as it is presented and explained hereafter, the method is completely revised in terms of temperature retrieval. Only a short summary of what is taken from the previously published method will be given here. The density and the background parameters are retrieved simultaneously from the solar occultation data, using the Optimal Estimation (OE) method developed by Rodgers [Rodgers, 1990, 2000]. The background parameters are fifth-order polynomial expressions that fit the backgrounds of each spectrum. They account for the absorption of all nonmolecular species, like aerosols [Wilquet *et al.*, 2012], or any molecule that has a structure broader than a SOIR diffraction order.

[10] The useful altitude range varies depending on the order studied and the targeted species. The maximum altitude corresponds to the tangent altitude at which absorption structures appear in the spectra. The minimum altitude is obtained when the absorption lines are saturated. The same approximation in terms of inversion scheme as in the onion peeling method is used to discretize the atmosphere: the

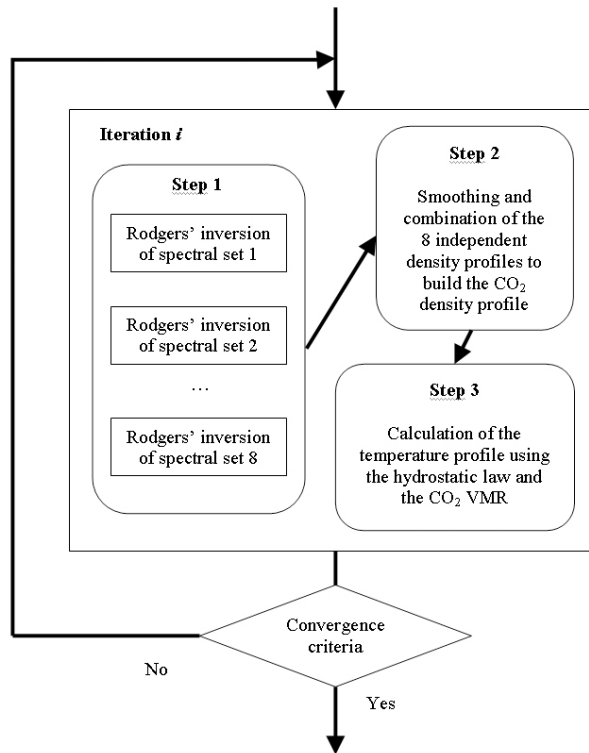


Figure 1. Working principle of the iterative inversion scheme. At each iteration, as a first step, the eight sets of spectra are inverted using the Asimat algorithm without fitting the temperature. Then, the eight independent CO₂ density profiles are recombined into one single smooth profile. The last step consists in calculating the temperature profile using the hydrostatic law and the CO₂ VMR from the Keating and Zasova models [Keating *et al.*, 1985; Zasova *et al.*, 2007, 2006]. The convergence criteria are used to check if more iterations are needed.

atmosphere is assumed to be spherically homogeneous at each altitude level [Mahieux *et al.*, 2010; Vandaele *et al.*, 2008]. This is an approximation, as it is known that the atmosphere undergoes density variations across the terminator, with larger densities on the dayside than the nightside at same altitude levels. However, the steepness and the shape of these gradients are currently unknown. Attempts have been made to introduce a horizontal dependency of the density orthogonally to the terminator. This does not change the shape of the retrieved vertical density profiles, but only scales the whole density profile by a factor proportional to the introduced dependency. For this reason, the density gradient is not taken into account in the following, though it will be further investigated in the future.

[11] In the companion paper [Mahieux *et al.*, 2010], we claimed that the rotational temperature could be derived directly from the spectra, using the rotational structure of the CO₂ absorption bands which are resolved. However, it has been observed that this approach leads to incorrect temperature profiles [Mahieux *et al.*, 2011]. The envelope of the rotational structure as seen in the measured spectra is modulated by the instrument AOTF bandpass function during the acquisition process. The shape of this function is

unfortunately slightly broader to the rotational structure envelope, and obscures the dependency of the measured rotational envelope on gas rotational temperature. The retrieved temperature profiles obtained using the Rodgers method were unchanged from the a priori temperature profiles, implying that no information on the local temperature could be gained from measurements. In addition, density and temperature profiles resulting from the inversion did not verify hydrostatic equilibrium, which is not physically valid. Altogether, this clearly indicates that the temperature profiles are not directly retrievable, using the rotational information contained in the spectra.

[12] In order to overcome this issue, a global iterative approach is now considered, in which each iteration is performed in three steps, see the diagram in Figure 1. First, the CO₂ density is calculated using the previous iteration temperature profile, then a new temperature profile is obtained from the new CO₂ density profile: at each iteration, the Asimat algorithm is applied with the temperature profile fixed, on all the simultaneous sets of spectra from all orders and bins in which CO₂ is measured. In a second step, the CO₂ density profiles are combined in a single one, and in a third step the hydrostatic equilibrium equation is used to derive the new temperature profile.

[13] In order to illustrate the method, let us consider an orbit for which the four diffraction orders are dedicated to CO₂ measurements which cover the whole altitude range, i.e., between 85 and 155 km of altitude. The Asimat algorithm is run on the 8 sets of spectra (one spectrum per bin per order). The initial temperature profile is chosen as the Zasova model [Zasova *et al.*, 2007, 2006] below 100 km and the Keating model [Keating *et al.*, 1980] above 140 km. The inversions result in a set of eight CO₂ density vertical profiles. These independent density profiles are combined into a single one, using a moving linear mean square regression, weighted by the error of each individual density value and that considers all the points located within one scale height of altitude. One single smooth CO₂ recombined density profile is thus obtained. SOIR typical vertical sampling varies with the latitude of the measurement: 1 km above 70°N, 500 m between 40° and 70°N, and from 1 to 4 km south of 40°N, with the largest values at the South Pole. Tangent altitudes vary slightly among the eight data set spectra requiring interpolation of the atmospheric results on a new altitude scale. An altitude step of 1 km has been chosen. Smaller altitude steps were also considered, but this step did not influence the results.

[14] At the end of each iteration, a new temperature profile is calculated from the hydrostatic equation and the ideal gas law using the CO₂ vertical profile:

$$\begin{cases} dp(z) = -\rho(z) \cdot MM(z) \cdot g(z) \cdot dz \\ g(z) = g_0 \cdot \left(\frac{R_{Venus}}{R_{Venus} + z} \right)^2 \\ p(z) = \rho(z) \cdot k_B \cdot T(z) \\ \rho_{CO_2}(z) = VMRCO_2(z) \cdot \rho(z) \end{cases} \\ \Rightarrow T(z) = - \frac{VMRCO_2(z) \cdot MM_{CO_2}}{k_B \cdot \rho_{CO_2}(z)} \cdot \int_{z_0}^z \frac{(\rho_{CO_2}(\bar{z}) - \rho_{CO_2}(z_0)) \cdot g(\bar{z})}{VMRCO_2(\bar{z})} \cdot d\bar{z} \quad (1)$$

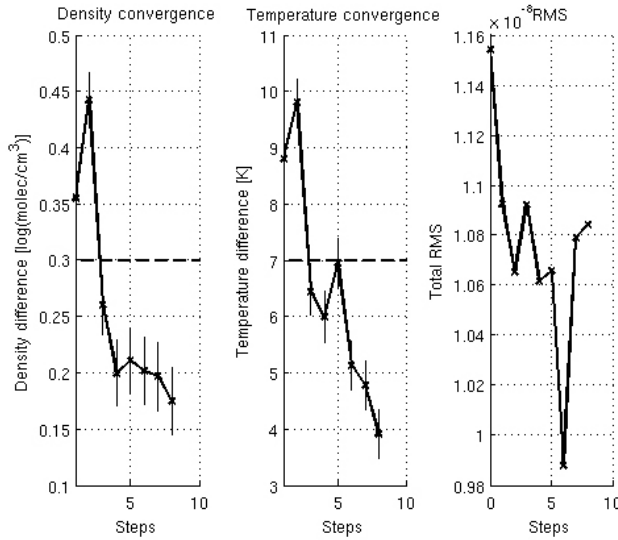


Figure 2. Illustration of the convergence of the atmospheric parameters iterative procedure for orbit 687.1. The (left) density convergence and (middle) temperature convergence are presented. The parameters that are plotted for both variables are the integrated difference between two successive profiles. The error bars represent the average density and temperature error. (right) The residual mean square summed on all the fitted spectra that are considered to build the profiles at each step of the occultation. The convergence criterion is set to 0.3 for the density logarithm and 7 K for the temperature, and is shown as the thick line in the left and middle panels. The convergence occurs after three steps. The further steps are displayed to show the stabilization, within the error bar. After 2 steps, the RMS is getting lower (see Figure 2, right).

where z is the altitude, z_0 is the reference altitude, $p(z)$ is the total pressure, $\rho_{CO_2}(z)$ is the CO₂ volume density and $\rho(z)$ is the total volume density, $VMR_{CO_2}(z)$ is the CO₂ VMR, MM_{CO_2} is the CO₂ molar mass (44.01 g/mol) and $MM(z)$ is the atmosphere molar mass, $g(z)$ is the Venus gravitational acceleration, g_0 is the Venus gravitational constant (8.87 m/s²), R_{Venus} is the Venus radius (6053.1 km), $T(z)$ is the temperature profile and k_B is the Boltzmann constant ($1.38 \cdot 10^{-23}$ J/K). The altitude step Δz chosen in the altitude scale equals to 1 km. The reference altitude z_0 is always taken as the altitude of the highest retrieved point. The CO₂ VMR is taken from the Keating [Keating *et al.*, 1980] and Zasova [Zasova *et al.*, 2007, 2006] models, as a function of altitude.

[15] Because CO₂ absorption cross sections (ACS) are temperature dependent, the Asimat algorithm is iteratively run on the 8 sets of measured spectra, considering the last temperature profile obtained. The convergence is assumed to be achieved when both recombined density and temperature profiles stabilize. In the present study we specify that the temperature difference between two successive iterations should be less than 7 K, and the density natural logarithm difference less than 0.3, both calculated as integrated difference on the whole profile. The evolution of those two convergence criteria is shown in Figure 2 for a typical observation (in this case, orbit 687.1–03/08/2008). The total

root mean square (RMS) value obtained by summing all residuals of all the spectra included in the retrieval (all orders, all bins, and all altitudes) is also shown in Figure 2. Considering the convergence criteria on the density and the temperature and allowing for the total RMS to stabilize to a low value, it can be seen that in the illustrated example, convergence is achieved after 3 steps. Typically, convergence is reached after 4 steps (3.93 ± 1.44). Figure 3 illustrates the evolution of the density and the temperature profiles during the iterative process. The density profile departs from initialization notably at 120–130 km altitudes, associated with a ~ 100 K variation in temperature over this altitude region.

[16] The hydrostatic equation is applied in the described method whether the measurements are taken above or below the homopause, since equation (1) considers the total density of the atmosphere. The homopause is located at an altitude of about 125 km on Venus or at a pressure level of 2.10^{-5} mbar [de Pater and Lissauer, 2001]. Below that level, in the homosphere, each species adopts the same scale height, which is given by the average molecular mass of the atmosphere, whereas above, in the heterosphere, molecular diffusion dominates over vertical mixing [Jacobson, 1999]; each individual species follows its own scale height.

[17] From equation (1), it can be seen that the temperature profile is dependent on the density value derived at the top of the profile: $\rho_{CO_2}(z_0)$. In order to study the influence of this parameter, the temperature profile has been calculated for density values at the top of the atmosphere varying between $\rho_{CO_2}(z_0) - 2 \cdot \sigma$ and $\rho_{CO_2}(z_0) + 2 \cdot \sigma$, with σ the density error at the top of the profile. The results are presented in Figure 4. The impact of the starting density remains below the retrieved temperature error bars, which indicates that the influence of this parameter does not affect much the temperature retrieval. However, the temperature profile is strictly reliable 10 km below the maximum altitude, which is located between 1 and 2 scale heights above the homopause altitude. The temperature profiles are robust below 140 km, while larger error bars are observed at higher altitude.

[18] Finally, knowing the temperature profile derived using the method described just above, and considering the CO₂ VMR from the models of Keating and Zasova [Keating *et al.*, 1985; Zasova *et al.*, 2007, 2006], which is the only information that could not be directly retrieved from the SOIR measurements, it is possible to derive the total atmospheric pressure and density and the scale height, $H(z)$:

$$\begin{cases} \rho(z) = \frac{\rho_{CO_2}(z)}{VMR_{CO_2}(z)} \\ p(z) = \rho(z) \cdot k_B \cdot T(z) \\ H(z) = \frac{k_B \cdot T(z)}{g(z) \cdot MM_{CO_2} \cdot VMR_{CO_2}(z)} \end{cases} \quad (2)$$

The converged CO₂ density and temperature profiles for two typical orbits (687.1 and 1567.1) are given in Figure 5 along with their respective typical errors. A North polar and an equatorial measurement are chosen, in order to show the influence of the vertical sampling on the profiles – see Table 1 for the exact location of the measurements. The vertical sampling of the polar orbit is much larger than for the equatorial orbit, around 500 m and 3 km respectively. In

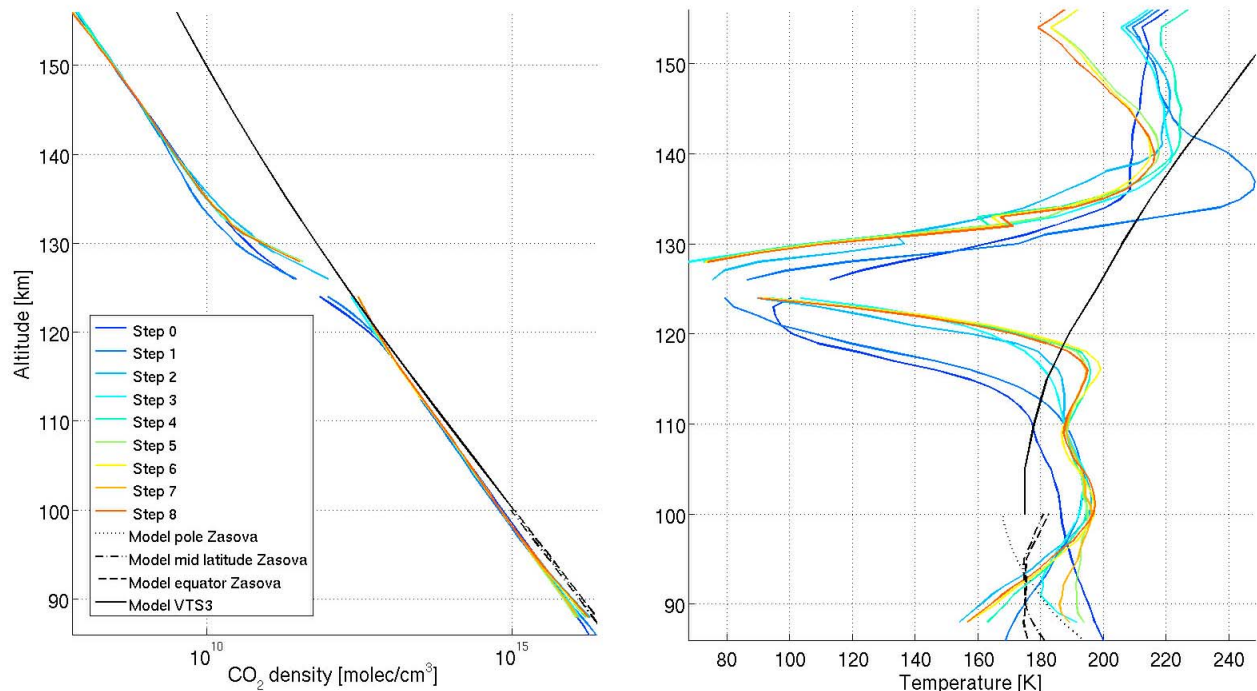


Figure 3. Convergence of the (left) CO₂ density and (right) temperature profiles for orbit 687.1 during the iterative procedure. The Zasova and the Keating models are presented as the black lines [Keating *et al.*, 1985; Zasova *et al.*, 2007, 2006]. The convergence occurred after 3 steps, both in terms of temperature and density (see Figure 2). The converged profiles are the thick green profiles. One step further is also displayed to show the stabilization of the derived profiles.

the top part of the figure, the two panels present the individual CO₂ density values covering the altitudes from 80 to 160 km, along with the averaged CO₂ vertical profile. The error level on the density for the two presented orbits is between 1 and 5%. The temperature profiles, in the bottom panels, are obtained from the CO₂ density profile using equation (1), assuming the hydrostatic equilibrium and the CO₂ VMR from the Keating and Zasova models. The error on the temperature, given by the gray envelopes, varies typically from 1 to 20 K and is higher when the slope in the CO₂ density varies rapidly or at high altitude where the CO₂ VMR has smaller values. The cold layer at the altitude of 110–140 km results from the change of curvature of the CO₂ density profile at the same altitude level.

4. Orbit Selection and Localization

[19] Although the SOIR data set now contains 478 observations (up to January 2012) from which 465 can be used to retrieve information on CO₂, only a subset has been considered in this study to define the Venus Atmosphere from SOIR measurements at the Terminator (VAST). Indeed we only considered the orbits for which CO₂ has been measured at least once at very high altitude, i.e., in which the strong ¹²C¹⁶O₂ absorption band at 3 μm is present. This corresponds to SOIR orders 160 to 166. This band is usually observed from an altitude as high as 165 km. Using this criteria, only 59 observations were considered. The selected measurements are obtained on AM or PM terminator sides

for a wide range of latitudes. In terms of time coverage, they were obtained during various occultation seasons (from OS 1 to OS 17) between 2006 and 2011. Figure 6 shows the localization in terms of orbit number, latitude and local solar time of the measurements. The fact that the local solar times displayed in Figure 6 are not equal to 6:00 A.M. or 6:00 P.M. when approaching to the pole is an artifact, and comes from the fact that the notion of local solar time becomes meaningless at these latitudes. This means that the only local solar time information that should be used is the terminator side, either AM or PM. Details of the selected orbits are summarized in Table 1. In the future, VAST developed here will be used as starting condition for the resolution of equation (1). The aim is to gradually incorporate new retrievals as they are obtained to refine the model.

[20] Due to the VEX orbit, two successive measurements, which occur on a 24 Earth hour basis, are taken at somewhat different latitudes on the same side of the terminator: there is a time-latitude gap between successive measurements, such that it is not easy to discriminate between time and latitude variations of the density or temperature profiles. In consequence, latitudinal and short-term trends should be considered with care, as they are intrinsically linked.

[21] Short-term CO₂ density variations for a given latitude region of the terminator are not considered in the current study, since they are removed by the use of a statistically large enough sample of profiles. Systematic long-term CO₂ density variations are not observed in the subset studied

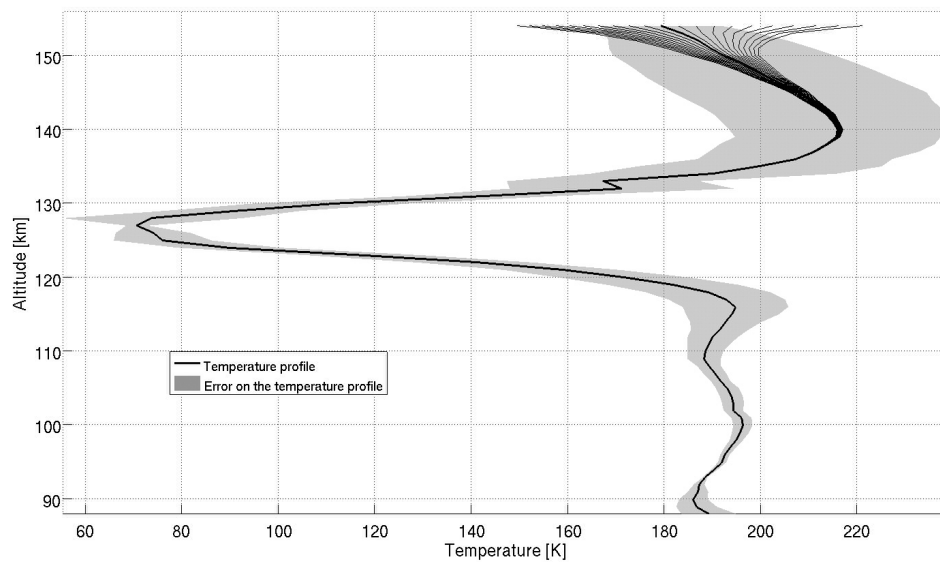


Figure 4. Influence of the initial density value on the derived temperature profile presented for orbit 687.1. The temperature profiles are calculated using the hydrostatic law for different initial density values, ranging from $\rho_{CO_2}(z_0) - 2 \cdot \sigma$ and $\rho_{CO_2}(z_0) + 2 \cdot \sigma$, with σ the density error on the maximum altitude point, around the density derived at the maximum altitude, $\rho_{CO_2}(z_0)$. The gray zone is the calculated error on the profile at convergence. It has typical values of 1 to 20 K. All the profiles starting from different initial temperatures align below two scale heights, which corresponds to 10 km at this altitude, and remain within the error bar of the converged profile at lower altitudes.

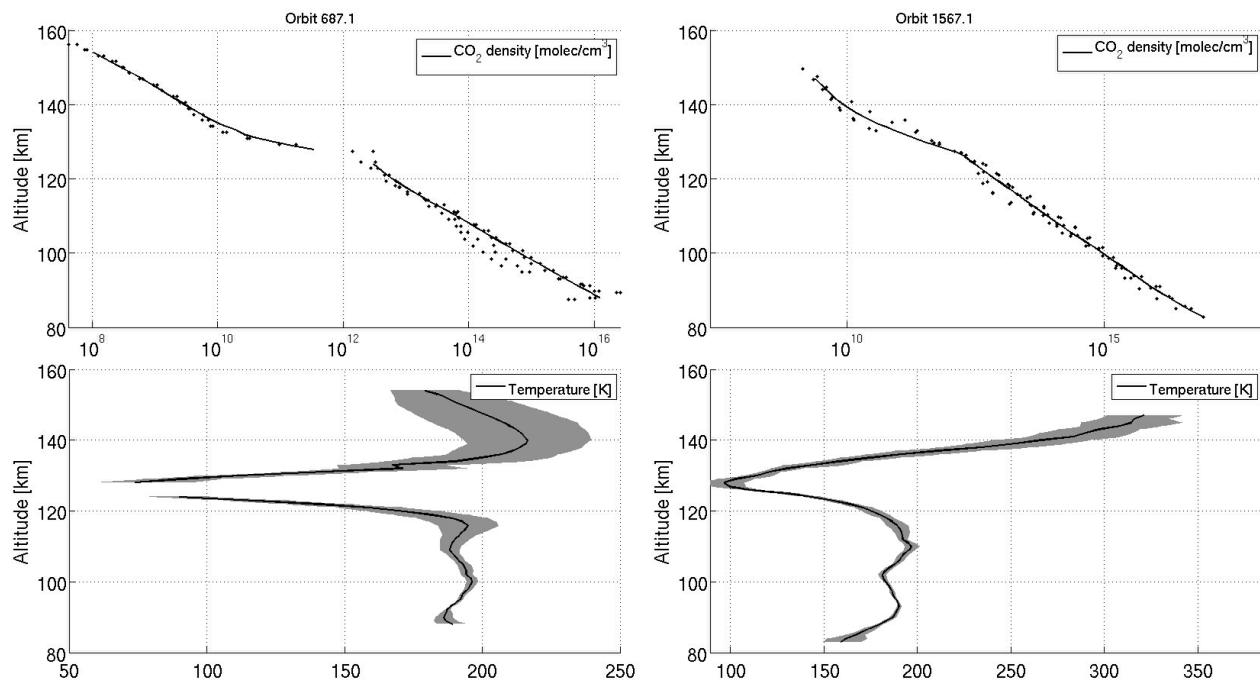


Figure 5. Example of two sets of profiles: (left) a North polar measurement (orbit 687.1) and (right) an equatorial measurement (orbit 1567.1). The main difference between the two profiles resides in the vertical resolution and the number of measurement points, which are lower when going to Southern latitudes. (top) In the CO₂ density panels, the points are the retrieved individual density values, and the black line is the averaged profile. The error ranges between 1 and 5%. (bottom) In the temperature panels, the gray envelope is the error on the temperature. Typical temperature error values are 1 to 20 K.

Table 1. List of the 59 Occultations Studied in This Work^a

| Orbit | Date (DD/MM/YY) | OS | LST (Hour) | Lat (Deg) | Lon (Deg) | CO ₂ Orders | | | |
|--------|-----------------|----|------------|-----------|-----------|------------------------|---------|---------|---------|
| | | | | | | Order 1 | Order 2 | Order 3 | Order 4 |
| 35.1 | 26/05/06 | 1 | 5.205 | 76.7 | 306 | 166 | 167 | | |
| 361.1 | 17/04/07 | 4 | 6.862 | 79.8 | 207 | 112 | 147 | 149 | 166 |
| 593.1 | 05/12/07 | 6 | 6 | 2 | 215 | 112 | 147 | 149 | 162 |
| 597.2 | 09/12/07 | 6 | 6 | 64 | 222 | 111 | 149 | 161 | 119 |
| 667.1 | 17/02/08 | 7 | 18 | 80 | 258 | 112 | 149 | 166 | |
| 669.1 | 19/02/08 | 7 | 19 | 81 | 262 | 112 | 149 | 166 | |
| 671.1 | 21/02/08 | 7 | 19 | 82 | 266 | 112 | 149 | 166 | |
| 674.1 | 24/02/08 | 7 | 19 | 84 | 271 | 112 | 149 | 166 | |
| 675.1 | 25/02/08 | 7 | 19 | 84 | 272 | 112 | 149 | 166 | |
| 677.1 | 27/02/08 | 7 | 19 | 85 | 274 | 112 | 149 | 166 | |
| 679.1 | 29/02/08 | 7 | 20 | 86 | 273 | 112 | 149 | 166 | |
| 681.1 | 02/03/08 | 7 | 20 | 87 | 270 | 112 | 149 | 166 | |
| 684.1 | 05/03/08 | 7 | 22 | 88 | 254 | 112 | 149 | 166 | |
| 685.1 | 06/03/08 | 7 | 23 | 88 | 245 | 112 | 149 | 166 | |
| 686.1 | 07/03/08 | 7 | 24 | 88 | 235 | 112 | 149 | 166 | |
| 687.1 | 08/03/08 | 7 | 1 | 88 | 225 | 112 | 149 | 166 | |
| 688.1 | 09/03/08 | 7 | 1 | 88 | 216 | 112 | 149 | 166 | |
| 689.1 | 10/03/08 | 7 | 2 | 87 | 209 | 149 | 166 | | |
| 690.1 | 11/03/08 | 7 | 3 | 87 | 204 | 149 | 166 | | |
| 691.1 | 12/03/08 | 7 | 3 | 86 | 201 | 149 | 166 | | |
| 693.1 | 14/03/08 | 7 | 4 | 86 | 197 | 134 | 149 | 166 | |
| 695.1 | 16/03/08 | 7 | 4 | 84 | 197 | 149 | 166 | | |
| 697.1 | 18/03/08 | 7 | 4 | 83 | 198 | 149 | 166 | | |
| 699.1 | 20/03/08 | 7 | 5 | 82 | 201 | 149 | 166 | 178 | |
| 703.1 | 24/03/08 | 7 | 5 | 78 | 208 | 112 | 149 | 166 | |
| 705.1 | 26/03/08 | 7 | 5 | 76 | 212 | 149 | 166 | | |
| 706.1 | 27/03/08 | 7 | 5 | 75 | 214 | 149 | 166 | | |
| 709.1 | 30/03/08 | 7 | 5 | 70 | 220 | 112 | 149 | 166 | |
| 710.1 | 31/03/08 | 7 | 6 | 68 | 222 | 117 | 118 | 149 | 166 |
| 710.2 | 31/03/08 | 7 | 6 | 18 | 217 | 149 | 166 | 121 | 171 |
| 711.1 | 01/04/08 | 7 | 6 | 60 | 220 | 121 | 149 | 166 | 171 |
| 711.2 | 01/04/08 | 7 | 6 | 26 | 220 | 149 | 166 | 121 | 171 |
| 1121.1 | 16/05/09 | 11 | 19 | 83 | 212 | 161 | 162 | | |
| 1124.1 | 19/08/09 | 11 | 18 | -44 | 234 | 121 | 149 | 166 | 171 |
| 1126.1 | 21/08/09 | 11 | 18 | -52 | 240 | 149 | 166 | | |
| 1128.1 | 23/08/09 | 11 | 18 | -61 | 248 | 149 | 161 | 162 | 166 |
| 1130.1 | 25/08/09 | 11 | 18 | -69 | 255 | 149 | 166 | | |
| 1132.1 | 27/08/09 | 11 | 18 | -77 | 264 | 149 | 166 | | |
| 1137.1 | 01/06/09 | 11 | 1 | 88 | 166 | 160 | 163 | 164 | 165 |
| 1139.1 | 03/06/09 | 11 | 7 | -75 | 91 | 121 | 149 | 166 | 171 |
| 1141.1 | 05/06/09 | 11 | 6 | -67 | 100 | 149 | 166 | | |
| 1154.1 | 18/06/09 | 11 | 6 | -8 | 144 | 149 | 161 | 162 | 166 |
| 1252.1 | 24/09/09 | 12 | 5 | -74 | 95 | 149 | 164 | 165 | 166 |
| 1254.1 | 26/09/09 | 12 | 6 | -65 | 98 | 149 | 166 | 167 | 168 |
| 1256.1 | 28/09/09 | 12 | 6 | -57 | 103 | 121 | 149 | 166 | 171 |
| 1381.2 | 31/01/10 | 13 | 6 | 13 | 126 | 149 | 160 | 165 | |
| 1461.1 | 21/04/10 | 14 | 17 | 85 | 205 | 117 | 148 | 160 | 165 |
| 1462.1 | 22/04/10 | 14 | 18 | -48 | 192 | 148 | 156 | 166 | |
| 1464.1 | 24/04/10 | 14 | 16 | 86 | 224 | 111 | 150 | 160 | 165 |
| 1465.1 | 25/04/10 | 14 | 18 | -60 | 200 | 111 | 149 | 160 | 166 |
| 1467.1 | 27/04/10 | 14 | 15 | 87 | 248 | 149 | 150 | 156 | 166 |
| 1469.1 | 29/04/10 | 14 | 19 | -76 | 207 | 112 | 148 | 156 | 166 |
| 1480.1 | 10/05/10 | 14 | 9 | 87 | 31 | 141 | 150 | 156 | 165 |
| 1565.1 | 03/08/10 | 15 | 18 | 75 | 149 | 148 | 165 | 155 | 179 |
| 1567.1 | 05/08/10 | 15 | 18 | -11 | 159 | 141 | 149 | 156 | 166 |
| 1581.1 | 19/08/10 | 15 | 21 | 87 | 155 | 148 | 165 | 155 | 179 |
| 1798.1 | 24/03/11 | 17 | 19 | 82 | 140 | 118 | 141 | 156 | 167 |
| 1802.1 | 28/03/11 | 17 | 19 | 85 | 142 | 141 | 156 | 167 | |
| 1804.1 | 30/03/11 | 17 | 20 | 86 | 142 | 118 | 141 | 156 | 167 |

^aOS is the occultation season number, LST is the mean local solar time of the measurement in hour, Lat is the mean latitude in degrees, and Lon is the mean longitude in degrees. The decimal after the orbit number represents the measurement number of the day. The orders used to derive information on the CO₂ density and temperature profiles are also indicated. The orders 121 (2704 to 2727 cm⁻¹), 134 (2995 to 3020 cm⁻¹), 171 (3822 to 3854 cm⁻¹), 176 to 180 (3933 to 4057 cm⁻¹) give the CO₂ density at low altitudes (70 to 90 km). Midaltitude (80 to 120 km) CO₂ density is derived from orders 112 (2503 to 2525 cm⁻¹), 117 and 118 (2615 to 2637 cm⁻¹), 141 (3151 to 3178 cm⁻¹), 147 to 150 (3285 to 3381 cm⁻¹). The orders 155 and 156 (3464 to 3516 cm⁻¹) give information on the CO₂ density at high altitudes (100 to 140 km), and orders 160 to 168 (3576 to 3787 cm⁻¹) at very high altitudes (120 to 170 km).

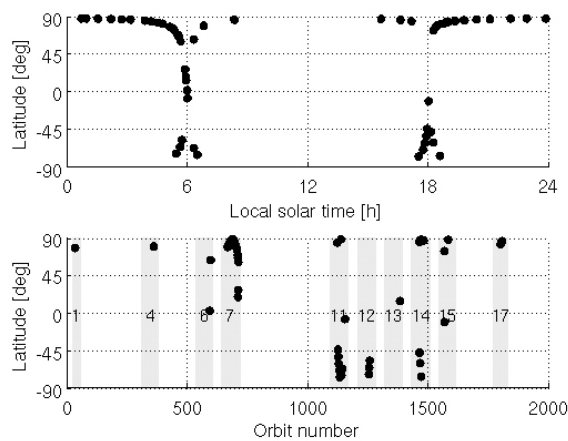


Figure 6. Localization of the orbit data set considered in the study. (top) The local solar time of the measurement as a function of the latitude. (bottom) The orbit number as a function of the latitude of the measurement. The occultation seasons considered are in gray, and their number is also indicated.

here. These variations could obviously influence the model, and will be investigated further in the future.

5. Carbon Dioxide Density and Temperature Profiles

[22] The carbon dioxide density and temperature profiles are presented in Figure 7 for the whole set. The error bars are not displayed to ensure readability of the figure.

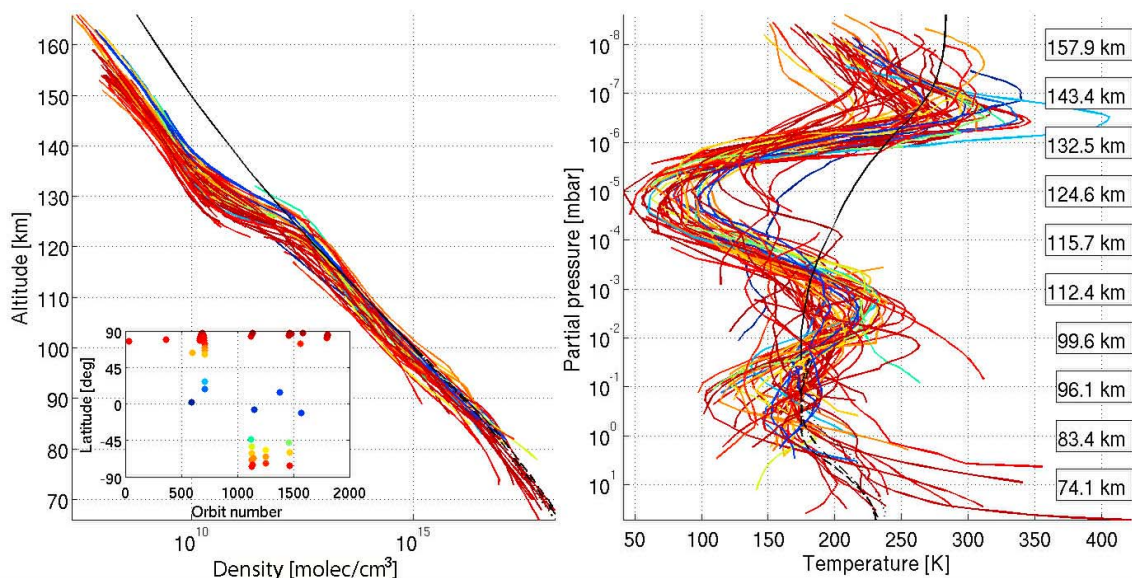


Figure 7. (left) CO₂ density profiles and (right) CO₂ temperature profiles of the orbit data set considered in this study. The inset panel gives the measurement latitude and the orbit number. The density profiles are given as a function of the altitude, and the temperature profiles are given as a function of the total pressure, with the altitude given on the right side as an indication. The color is the absolute latitude. High-latitude measurements are reddish, while equatorial measurements are bluish. The black lines are the density and temperature values of the Keating [Keating *et al.*, 1980] (plain line) and Zasova models [Zasova *et al.*, 2007, 2006], for different latitudes (dashed is 0°, dash-dotted is 45° and dotted is 90°).

[23] The density profiles all show the same shape, with a small yet systematic latitudinal dependency. They present a change of slope – a curvature – in the logarithmic scale around 120–140 km of altitude. The steepness of this gradient may change slightly from one orbit to another, and appears to also depend on latitude. Also, Figure 7 indicates that a global variability of the CO₂ density profiles (within a factor 10) is observed as a function of time and/or latitude. At constant density, the variations are equivalent to 2 scale heights (the scale height H is approximately 3 to 5 km). The general relative error on the density profiles is 1% to 10%, except in the region of the curvature change (120–140 km) where larger errors are observed, 10% to 40%.

[24] The temperature profiles are given as a function of total pressure to ensure consistent comparison between the different curves, in other terms to remove the influence of the observed local variations in the CO₂ density. The change of slope in the density profiles observed in Figure 7 corresponds to a temperature minimum in the 10⁻⁵ mbar region (120–130 km of altitude), with low temperatures between 60 and 110 K. This minimum is surrounded by two temperature maxima, located in the 5·10⁻⁷ mbar region or 130–140 km of altitude range (200–350 K) and the 5·10⁻³ mbar region or 100–110 km of altitude range (180–250 K). For a given pressure level, the temperature profiles also show variability of the order of 50 K, at all altitudes. At constant temperature, the variations are also equivalent to 2 scale heights (around 3 to 5 km). The error bars for the temperature profiles vary between 2 and 10 K below 120 km and between 10 and 60 K above 120 km. These values are directly linked to the error on the density profiles and to the value of the CO₂ VMR obtained from the

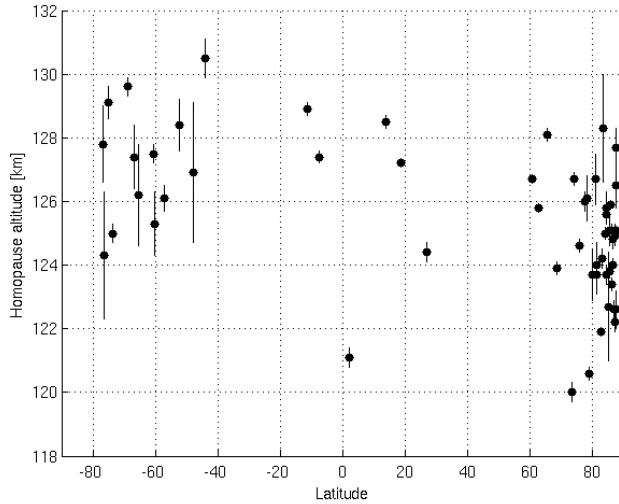


Figure 8. Homopause altitudes derived from the SOIR measurements, together with the error values. The altitude of the homopause derived from the SOIR data varies between 120 and 132 km.

Keating and Zasova models, through the hydrostatic equilibrium in equation (1). Larger temperature errors are observed at high altitude due to the lower values of the CO₂ VMR.

[25] The CO₂ density profiles and the temperature profiles are compared in Figure 7 to the Keating and Zasova models. In terms of density, the agreement is good at altitudes lower than 120 km, but the model does not reproduce the observed CO₂ density drop measured by the SOIR instrument. This is reflected in the temperature profiles, as the measured cold layer in the 10⁻⁵ mbar region is not present in the Keating and Zasova models [Keating *et al.*, 1980; Zasova *et al.*, 2007, 2006]. At higher pressure level (lower altitudes), the agreement between the model and the SOIR temperatures is better, but differences can reach up to 50 K.

6. CO₂ Homopause Altitude

[26] The homopause is the altitude level at which the molecular diffusion and eddy diffusion processes are of the same order of magnitude. Above the homopause, each species assumes its own scale height based on its own molecular mass. The composition of the atmosphere varies with altitude even in the homosphere, the difference with the heterosphere being that all species share the same hydrostatic scale height, computed from the local mean molecular mass.

[27] The molecular diffusion coefficient of CO₂ (D_{CO_2}) is obtained using the relations [Jacobson, 1999]:

$$D_{CO_2} = \frac{3 \cdot 10^{-2} \cdot \pi \cdot \sqrt{2}}{16} \cdot l_{CO_2} \cdot v_{CO_2}^{th} \quad \text{with } l = \frac{1}{Q_{CO_2} \cdot \rho_{CO_2}} \quad \text{and} \quad (3)$$

$$v_{CO_2}^{th} = \sqrt{\frac{3 \cdot k_B \cdot T \cdot N_{Av}}{MM_{CO_2}}}$$

where l_{CO_2} is the free mean molecular path, $v_{CO_2}^{th}$ the mean molecular thermal speed, Q_{CO_2} the CO₂ effective

cross section (0.52 nm²) and N_{Av} the Avogadro number (6.02·10²³ molec).

[28] The eddy coefficient is calculated using [Brecht *et al.*, 2012; von Zahn *et al.*, 1979, 1980]:

$$K = \frac{5.5 \cdot 10^{12}}{\sqrt{\rho}} \quad (4)$$

The homopause level corresponds to the altitude where the molecular diffusion coefficient equals the eddy diffusion coefficient [Jacobson, 1999]. The derived homopause altitude varies between 124 and 134 km as shown in Figure 8. This is in agreement with the literature [de Pater and Lissauer, 2001; Jacobson, 1999; von Zahn *et al.*, 1980]. For example, de Pater and Lissauer, 2001 reported values at 2·10⁻⁵ mbar, which corresponds to 120 to 132 km. A large altitude variability is observed, corresponding to two scale heights, but no latitudinal trend.

7. Venus Atmosphere From SOIR Measurements at the Terminator (VAST)

[29] In order to study the global distribution of the latitudinal parameters, the profiles are grouped in latitude zones, and the mean and standard values of the atmospheric parameters are computed at each altitude level. The latitude groups are summarized in Table 2. They have been chosen such that each group is statistically meaningful, i.e., that the number of measurements is statistically reliable. For that reason, the first two zones are 30 degrees large while above 60°, zones of 10° were considered. In the present study, symmetry in terms of latitude with respect to the equator is assumed, as it has been observed by the VIRTIS instrument on board Venus Express [Migliorini *et al.*, 2012]. Global circulation modeling predicts different wind and dynamics characteristics at the AM and PM sides of the terminator that should be reflected on density and temperature [Brecht, 2011]. However, symmetry between the morning and evening sides of the terminator has been assumed in this study. This is justified by the fact that no systematic variations were observed either in terms of latitude or terminator side on the measurements investigated in this data set. This observation will be verified in the future, considering new measurements campaigns. These hypotheses also ensure a statistically valid number of measurements in each latitude region, which would not be the case if AM and PM measurements had to be considered separately.

[30] VAST profiles for the different latitude regions are shown in Figure 9 for the CO₂ density and in Figures 10

Table 2. Characteristics of the Different Latitude Zones Defined in VAST^a

| Latitude Min (deg) | Latitude Max (deg) | Number of Orbits | Altitude Min (km) | Altitude Max (km) |
|--------------------|--------------------|------------------|-------------------|-------------------|
| 0 | 30 | 6 | 82 | 165 |
| 30 | 60 | 4 | 78 | 161 |
| 60 | 70 | 9 | 81 | 168 |
| 70 | 80 | 11 | 73 | 168 |
| 80 | 90 | 29 | 62 | 161 |

^aEach group is characterized by a minimum and maximum latitude. The numbers of orbits, and the corresponding minimum and maximum probed altitudes of each group, are also indicated.

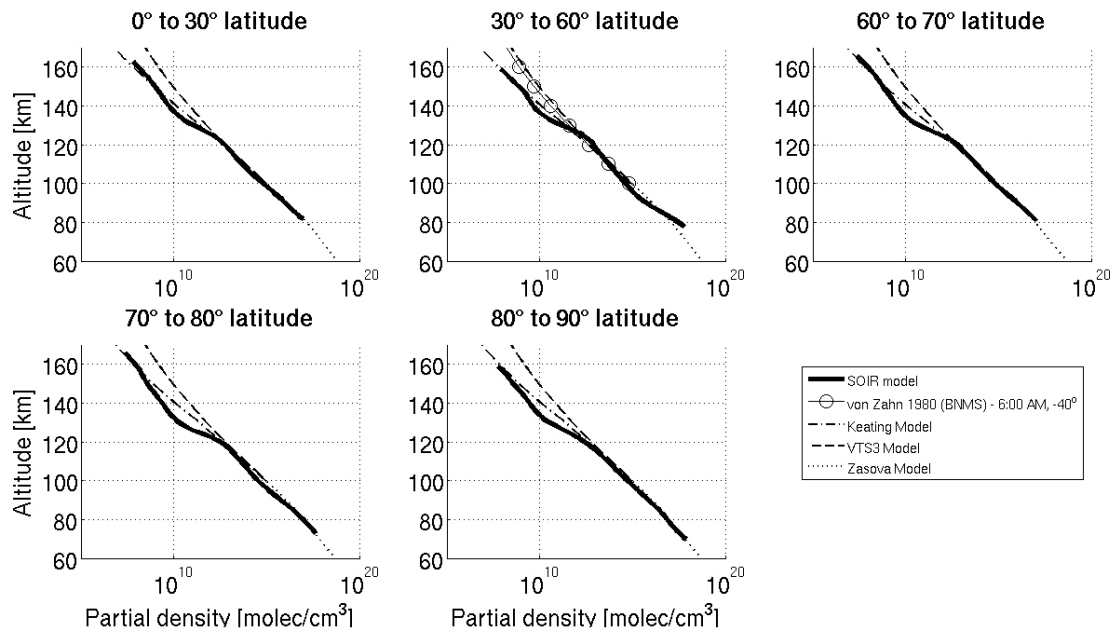


Figure 9. VAST CO₂ density profiles in function of altitude for the different latitude regions defined in Table 2. The thick line represents the VAST data; the confidence ranges between 1 and 5%. The Keating model [Keating *et al.*, 1980] is illustrated by the thin dash-dotted line, the Zasova model is illustrated by the plain black line [Zasova *et al.*, 2007, 2006], and the VTS3 model [Hedin *et al.*, 1983] is illustrated by the thin dashed line. The density profile obtained by Pioneer Venus is also given [von Zahn *et al.*, 1980].

to 14 for the temperature. In terms of CO₂ density, below 100 km VAST CO₂ density agrees with the Zasova model [Zasova *et al.*, 2007, 2006]. Above 100 km, VAST agrees better with the Keating model, based on the Pioneer Venus measurements [Keating *et al.*, 1980], whereas the temperature profiles are more consistent with the VTS3 model [Hedin *et al.*, 1983]. VAST CO₂ densities have also been

compared to those from von Zahn *et al.* [1980] in Figure 9. The Pioneer Venus data were taken in the Southern hemisphere (−40°), close to the morning side of the terminator. There is a good agreement from 100 to 130 km between the two data sets, but the Pioneer Venus data do not show the same pronounced gradient change at 125 km nor the lower densities observed by the SOIR instrument above. The

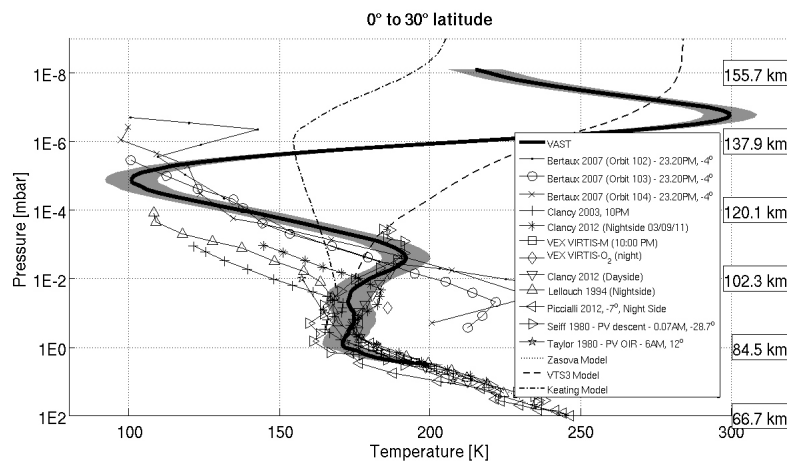


Figure 10. VAST temperature profiles in function of the total pressure in the 0 to 30° latitude region. The altitude levels are given as indications in the boxes. The thick line represents the VAST data; the gray envelope is its confidence range. The Keating model [Keating *et al.*, 1980] is illustrated by the thin dash-dotted line, the Zasova model is illustrated by the plain black line [Zasova *et al.*, 2007, 2006], and the VTS3 model [Hedin *et al.*, 1983] is illustrated by the thin dashed line. Different measurements from the literature, from ground-based or spacecraft measurements, are also indicated [Bertaux *et al.*, 2007b; Clancy *et al.*, 2003, 2012; Lellouch *et al.*, 1994; Piccialli *et al.*, 2012; Seiff *et al.*, 1980; Taylor *et al.*, 1980, and references therein]. The local solar times are given when they are known.

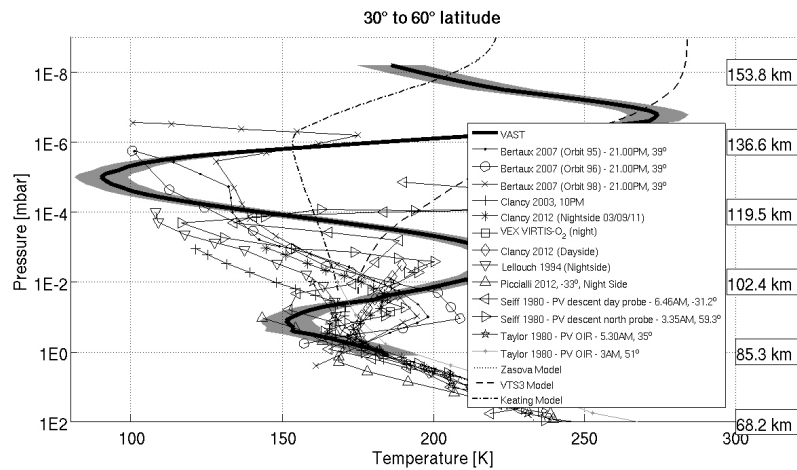


Figure 11. VAST temperature profiles in function of total pressure in the 30 to 60° latitude region. The altitude levels are given in the boxes. The thick line represents the VAST data; the gray envelope is its confidence range. The Keating model [Keating *et al.*, 1980] is illustrated by the thin dash-dotted line, the Zasova model is illustrated by the plain black line [Zasova *et al.*, 2007, 2006], and the VTS3 model [Hedin *et al.*, 1983] is illustrated by the thin dashed line. Different measurements from the literature, from ground-based or spacecraft measurements, are also indicated [Bertaux *et al.*, 2007b; Clancy *et al.*, 2003, 2012; Lellouch *et al.*, 1994; Piccialli *et al.*, 2012; Seiff *et al.*, 1980; Taylor *et al.*, 1980, and references therein]. The local solar times are given when they are known.

difference between the two models, VTS3 and Keating, at higher altitudes is striking and clearly indicates that observations performed by SOIR can be accounted for. The region between 120 and 140 km in which SOIR observations show a pronounced change in curvature is not reproduced by any of the models, but this is no surprise since both the Keating and the VTS3 models have been considered to start at 140 km, even if they return data down to 100 km. Nothing on this region can therefore be ascertained from these models. However, similar changes of curvature

of the CO₂ density in the 120 to 130 km of altitude are reproduced by Venus Thermospheric General Circulation Model (VTGCM) [Bougher *et al.*, 1988; Brecht *et al.*, 2012; Parkinson, private communication, 2012]. Detailed simulations by VTGCM of typical terminator profiles, such as those observed by SOIR, are currently under investigation.

[31] In the next paragraphs, VAST temperature profiles are compared to previously measured temperature profiles, for each latitude region. These are represented by different symbols in each plot of Figures 10 to 14, where they are

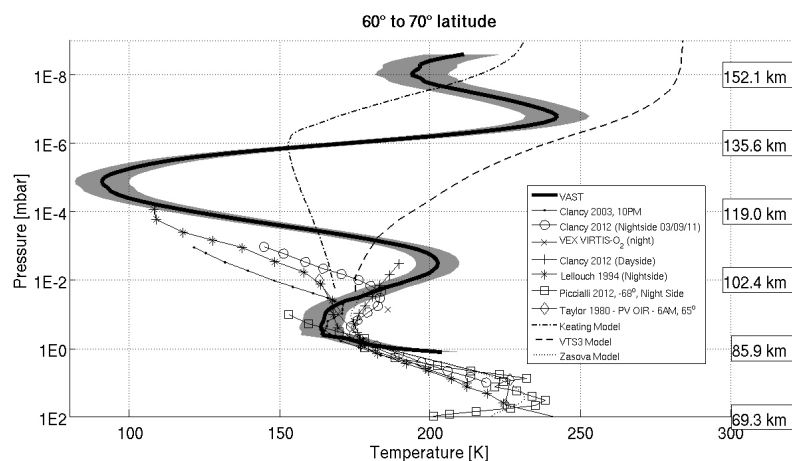


Figure 12. VAST temperature profiles in function of total pressure in the 60 to 70° latitude region. The altitude levels are given in the boxes. The thick line represents the VAST data; the gray envelope is its confidence range. The Keating model [Keating *et al.*, 1980] is illustrated by the thin dash-dotted line, the Zasova model is illustrated by the plain black line [Zasova *et al.*, 2007, 2006] and the VTS3 model [Hedin *et al.*, 1983] is illustrated by the thin dashed line. Different measurements from the literature, from ground-based or spacecraft measurements, are also indicated [Clancy *et al.*, 2003, 2012; Lellouch *et al.*, 1994; Piccialli *et al.*, 2012; Taylor *et al.*, 1980]. The local solar times are given when they are known.

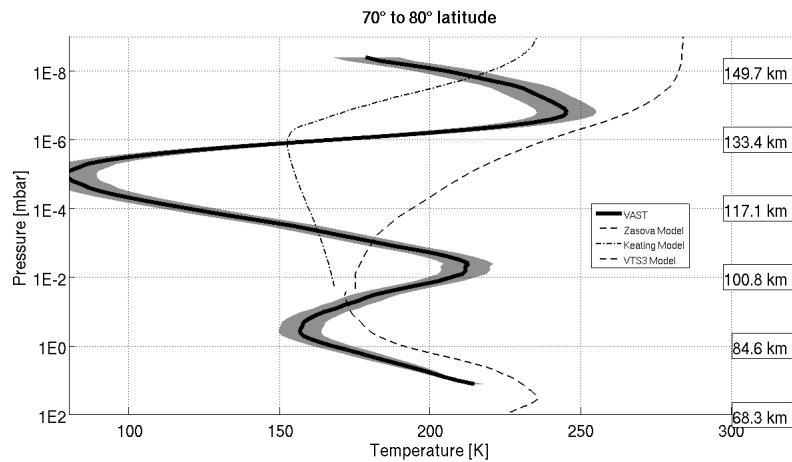


Figure 13. VAST for the temperature profiles in function of total pressure in the 70 to 80° latitude region. The altitude levels are given in the boxes. The thick line represents the VAST data; the gray envelope is its confidence range. The Keating model [Keating *et al.*, 1980] is illustrated by the thin dash-dotted line, the Zasova model is illustrated by the plain black line [Zasova *et al.*, 2007, 2006] and the VTS3 model [Hedin *et al.*, 1983] is illustrated by the thin dashed line.

placed in the corresponding figure when the latitude of the measurement is available. For most of the ground based measurements, the exact latitude and local solar time are not always specified or well characterized, as the field of view of the observing instrument often covers a wide range of latitudes and longitudes. For this reason, they are compared to midlatitudes measurements only – from the equator to 60°, in Figures 10 to 12. For all latitude regions, there is a good agreement in the 1 mbar to 10^{-2} mbar region (95 to 102 km region). The SOIR temperature measurements have recently been compared to simultaneous ground base measurements

by Sonnabend *et al.* [2012], and a good agreement (10 K) between the two data sets was reported.

[32] For the latitudinal region extending from the equator to 30° of latitude (see Figure 10), there is a good agreement with the SPICAV measurements that were obtained close to the subsolar point in the 10^{-2} to 10^{-5} mbar region (102 to 125 km) [Bertaux *et al.*, 2007b]. However, their inversion observed at 90–100 km is not present in the SOIR temperatures profiles, which show an inversion at a slightly higher altitude, around 110 km, with colder temperatures, around 190 K. The comparison with the Pioneer Venus

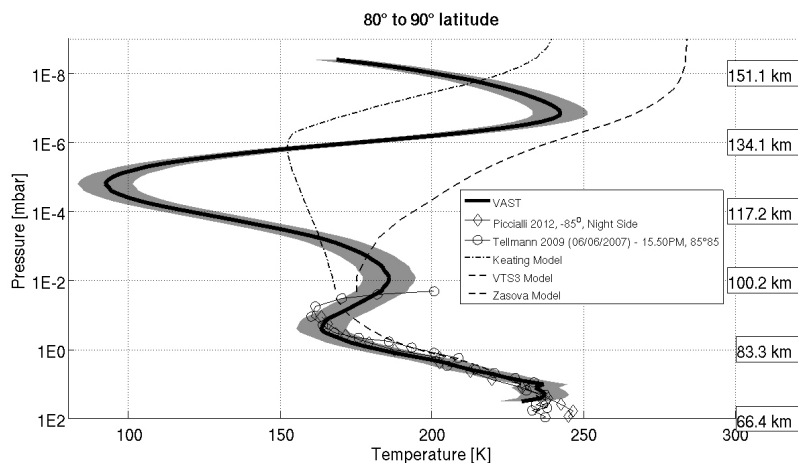


Figure 14. VAST temperature profiles in function of total pressure in the 80 to 90° latitude region. The altitude levels are given in the boxes. The thick line represents the VAST data; the gray envelope is its confidence range. The Keating model [Keating *et al.*, 1980] is illustrated by the thin dash-dotted line, the Zasova model is illustrated by the plain black line [Zasova *et al.*, 2007, 2006] and the VTS3 model [Hedin *et al.*, 1983] is illustrated by the thin dashed line. Different measurements from the literature, from ground-based or from spacecraft, are also indicated [Piccialli *et al.*, 2012; Tellmann *et al.*, 2009]. The local solar times are given when they are known.

descent probe from [Seiff *et al.*, 1980] is also in very good agreement in the 10 to 10^{-3} mbar region (80 to 105 km). Also, there is a good agreement with ground based measurements [Clancy *et al.*, 2003, 2012; Lellouch *et al.*, 1994], but also with the Pioneer Venus OIR measurement [Taylor *et al.*, 1980], with the measurements remaining within the SOIR error bars up to a pressure level of 10^{-2} mbar (100 km). However, there is a disagreement at higher altitudes, above the 10^{-2} mbar pressure level (100 km), where SOIR derives warmer temperatures. There is a source of uncertainty linked to the local solar time of some of the ground based measurements. Moreover they were not taken necessarily at the Venus terminator, like the SOIR measurements presented in this study. For example, all the SPICAV measurements [Bertaux *et al.*, 2007b] were obtained from the deep nightside of Venus. This might explain some of the observed discrepancies. Also, there is a large temperature variation of the SOIR data set (50 K) at all latitudes. Finally, a warm layer is observed at higher altitude corresponding to the 10^{-7} mbar pressure level or 140–145 km, which cannot be corroborated nor dismissed by existing ground-based or space observations.

[33] In the 30° to 60° latitude region presented in Figure 11, the SOIR mean profile is in agreement with some of the literature profiles in the 1 to 0.1 mbar region (80 to 90 km). At the 0.1 mbar level, the temperature inversion reported in most of the literature temperature profile is warmer (170 K) than the SOIR temperature (150 K) [Clancy *et al.*, 2003, 2012; Lellouch *et al.*, 1994; Seiff *et al.*, 1980; Taylor *et al.*, 1980]. Above the 0.1 mbar level, a warm layer is observed in the SOIR data around 10^{-3} mbar (112 km) with a temperature of 225 K, decreasing to a cold layer reaching 100 K at 10^{-5} mbar (125 km). Few of the literature profiles reported here show such a structure at these latitudes, except for the SPICAV measurements which also reach such cold temperature values – in the deep Venus nightside, but they do not show the same gradient nor coincide with the VAST profile [Clancy *et al.*, 2012]. VAST also agrees with the Keating and Zasova models at low altitude, at 1 mbar or 85 km. There is a warm layer observed at higher altitude corresponding to the 10^{-7} mbar pressure level or 140–145 km.

[34] In the 60° to 70° Lat region (Figure 12), the warm layer observed in VAST at the $5 \cdot 10^{-3}$ mbar pressure level (105 km) is colder (150 K) than in the 30° to 60° Lat region (180 K). VAST agrees with the ground based measurements [Clancy *et al.*, 2012; Lellouch *et al.*, 1994; Taylor *et al.*, 1980] and VeRa on board Venus Express measurements [Piccialli *et al.*, 2012] from the 1 mbar to 10^{-2} mbar pressure level (85 km to 100 km). At higher altitude, VAST shows a warm layer that is not reported in the literature at the $5 \cdot 10^{-3}$ mbar pressure level (105 km). Comparing the VAST temperature profile with the measurements obtained by Clancy *et al.* [2012] on the dayside and nightside of the Venus, the VAST minimum-maximum structure is also observed, such as in their nighttime profile, but VAST presents an intermediate regime between these two, with the maximum temperature located at higher altitude. The cold layer at the 10^{-5} mbar pressure level (125 km) reaches temperatures down to 90 K, which were already measured from ground based [Lellouch *et al.*, 1994] but at slightly lower altitude (10^{-4} mbar or 115 km) and on the Venus

nightside. A warm layer is also observed at higher altitude, 10^{-7} mbar or 140–145 km.

[35] In the 70° to 80° latitude region (see Figure 13), the profiles are not compared to ground based measurements as the latitude is too high, and ground based measurements have rather difficult access to these regions. Only the Keating and Zasova models are presented. There is a warm layer at the $8 \cdot 10^{-3}$ mbar (105 km) level, which located at slightly lower altitude than in the lower-latitude regions. The cold layer at the 10^{-5} mbar (125 km) level is observed at the same pressure level than in the other latitude regions, such as the warm layer located at 10^{-7} mbar level (140–145 km).

[36] In the 80° to 90° region (Figure 14), the SOIR temperature profile agrees almost perfectly, within the error bars, with the VeRa profile in the same latitude region [Tellmann *et al.*, 2009; Piccialli *et al.*, 2012], between 80 mbar and $3 \cdot 10^{-2}$ mbar (70 to 95 km). Above, the warm layer is located at 10^{-2} mbar (100 km), so slightly at lower altitude than at lower latitude, and the cold layer remains at the same pressure level (10^{-5} mbar or 125 km) and with the same temperature minimum (~ 90 K) [Clancy *et al.*, 2012]. The warm layer observed at higher altitude is also located at a pressure level of 10^{-7} mbar (140–145 km).

[37] The temperature decrease at the 10^{-3} to 10^{-5} mbar level region (110–130 km region) above the temperature maximum at $5 \cdot 10^{-3}$ mbar level (100–120 km region) has already been observed by the SPICAV instrument [Bertaux *et al.*, 2007b], and is observed on the Venus nightside by measurements made by VeRa [Piccioni *et al.*, 2009] on board Venus Express. The striking temperature minimum observed in the SOIR data set is always located at the same pressure level (10^{-5} mbar or 125 km), and reaches the same range of temperature (80–90 K).

[38] A comparison with nightside measurements obtained at different latitudes by VIRTIS on board Venus Express [Migliorini *et al.*, 2012] has also been carried out. The measurements described in that paper never occurred at the terminator, but at close local solar times (5:00 A.M. and 5:00 P.M.). The temperatures are close to the SOIR data presented here, between 190 and 220 K in the 1 to 100 mbar region. Also, there is a good agreement (less than 5 K difference) with the temperature profiles obtained by the VeRa instrument on board VEX at pressure levels between 100 and 0.1 mbar presented in Piccialli *et al.* [2012] at four different latitudes (-7° , -33° , -68° and -85° ; see Figures 10 to 14) in the Southern hemisphere, even if these measurements were obtained either at midnight or at 10:00 A.M.

8. Conclusions

[39] An atmospheric model for the Venus mesosphere and lower thermosphere has been constructed based on SOIR observations. Those correspond to solar occultation probing the altitude range from 70 to 170 km with a high vertical resolution. They cover a wide range of latitudes, but correspond all to the 6:00 A.M. and 6:00 P.M. local times, as all observations are performed at the terminator, either on its morning or its evening side. A subset of 59 observations has been considered, from which information on the CO₂ density and the temperature were derived. VAST (Venus Atmosphere from SOIR measurements at the Terminator) is defined on 5 latitudinal zones and provides CO₂ and total

densities and temperature as a function of the altitude. VAST has been compared to data available in the literature, and it was shown that, in particular, the temperature profiles are in good agreement with literature data at the lowest altitudes. A striking and never observed before cold layer is always observed at an altitude of 125 km.

[40] VAST will be further refined and improved with other CO₂ measurements, already recorded or obtained during future dedicated SOIR observation campaigns. The first step will be to analyze all observations already acquired allowing the determination of the CO₂ density and temperature, but which were not considered in this study because they did not cover a high enough altitude range. The model will also be further expanded with the inclusion of the vertical profiles of various trace gases observed by SOIR, such as H₂O and HDO [Fedorova et al., 2008], HCl, HF, CO [Vandaele et al., 2008], SO₂ [Belyaev et al., 2008, 2012].

[41] **Acknowledgments.** Venus Express is a planetary mission from the European Space Agency (ESA). We wish to thank all ESA members who participated in the mission, in particular, H. Svedhem and D. Titov. We thank our collaborators at IASB-BIRA (Belgium), Latmos (France), and IKI (Russia). We thank CNES, CNRS, Roskosmos, and the Russian Academy of Science. The research program was supported by the Belgian Federal Science Policy Office and the European Space Agency (ESA, PRODEX program, contracts C 90268, 90113, and 17645).

References

- Belyaev, D., O. Korablev, A. Fedorova, J. L. Bertaux, A. C. Vandaele, F. Montmessin, A. Mahieux, V. Wilquet, and R. Drummond (2008), First observations of SO₂ above Venus' clouds by means of solar occultation in the infrared, *J. Geophys. Res.*, *113*, E00B25, doi:10.1029/2008JE003143.
- Belyaev, D., F. Montmessin, J. L. Bertaux, A. Mahieux, A. Fedorova, O. Korablev, E. Marq, Y. Yung, and X. Zhang (2012), Vertical profiling of SO₂ and SO above Venus' clouds by SPICAV/SOIR solar occultations, *Icarus*, *217*(2), 740–751, doi:10.1016/j.icarus.2011.09.025.
- Bertaux, J. L., D. Nevejans, O. Korablev, E. Villard, E. Quémerais, E. Neefs, F. Montmessin, F. Leblanc, J. P. Dubois, and E. Dimarellis (2007a), SPICAV on Venus Express: Three spectrometers to study the global structure and composition of the Venus atmosphere, *Planet. Space Sci.*, *55*(12), 1673–1700, doi:10.1016/j.pss.2007.01.016.
- Bertaux, J. L., et al. (2007b), A warm layer in Venus' cryosphere and high altitude measurements of HF, HCl, H₂O and HDO, *Nature*, *450*, 646–649, doi:10.1038/nature05974.
- Bézar, B., J. P. Baluteau, A. Marten, and N. Coron (1987), The ¹²C/¹³C and ¹⁶O/¹⁸O ratios in the atmosphere of Venus from high-resolution 10- μ m spectroscopy, *Icarus*, *72*(3), 623–634, doi:10.1016/0019-1035(87)90057-1.
- Bougher, S. W., R. E. Dickinson, E. C. Ridley, and R. G. Roble (1988), Venus mesosphere and thermosphere. III. Three-dimensional general circulation with coupled dynamics and composition, *Icarus*, *73*, 545–573, doi:10.1016/0019-1035(88)90064-4.
- Brecht, A. (2011), *Tracing the Dynamics in Venus' Upper Atmosphere*, Univ. of Michigan, Ann Arbor.
- Brecht, A., S. W. Bougher, J. C. Gérard, and L. Soret (2012), Atomic oxygen distributions in the Venus thermosphere: Comparisons between Venus Express observations and global model simulations, *Icarus*, *217*(2), 759–766, doi:10.1016/j.icarus.2011.06.033.
- Clancy, R. T., and D. O. Muhleman (1991), Long-term (1979–1990) changes in the thermal, dynamical and compositional structure of the Venus mesosphere as inferred from microwave spectral line observations of ¹²CO, ¹³CO, and C¹⁸O, *Icarus*, *89*(1), 129–146, doi:10.1016/0019-1035(91)90093-9.
- Clancy, R. T., B. J. Sandor, and G. Moriarty-Schieven (2003), Observational definition of the Venus mesopause: Vertical structure, diurnal variation, and temporal instability, *Icarus*, *161*(1), 1–16, doi:10.1016/S0019-1035(02)00222-2.
- Clancy, R. T., B. Sandor, and G. Moriarty-Schieven (2008), Venus upper atmospheric CO, temperature, and winds across the afternoon/evening terminator from June 2007 JCMT sub-millimeter line observations, *Planet. Space Sci.*, *56*(10), 1344–1354, doi:10.1016/j.pss.2008.05.007.
- Clancy, R. T., B. Sandor, and G. Moriarty-Schieven (2012), Thermal structure and CO distribution for the Venus mesosphere/lower thermosphere: 2001–2009 inferior conjunction sub-millimeter CO absorption line observations, *Icarus*, *217*(2), 779–793, doi:10.1016/j.icarus.2011.05.032.
- de Pater, I., and J. Lissauer (2001), *Planetary Sciences*, Cambridge Univ. Press, Cambridge, U. K.
- Fedorova, A., et al. (2008), HDO and H₂O vertical distributions and isotopic ratio in the Venus mesosphere by Solar Occultation at Infrared spectrometer onboard Venus Express, *J. Geophys. Res.*, *113*, E00B22, doi:10.1029/2008JE003146.
- Fox, J. L., and W. T. Kasprzak (2007), Near-terminator Venus ionosphere: Evidence for a dawn/dusk asymmetry in the thermosphere, *J. Geophys. Res.*, *112*, E09008, doi:10.1029/2007JE002899.
- Hedin, A. E., H. B. Niemann, and W. T. Kasprzak (1983), Global empirical model of the Venus thermosphere, *J. Geophys. Res.*, *88*(A1), 73–83, doi:10.1029/JA088iA01p00073.
- Irwin, P. G., K. de Kok, A. Negro, C. Tsnag, C. F. Wilson, P. Drossart, G. Piccioni, D. Grassi, and F. W. Taylor (2008), Spatial variability of carbon monoxide in Venus' mesosphere from Venus Express/VIRTIS measurements, *J. Geophys. Res.*, *113*, E00B01, doi:10.1029/2008JE003093.
- Jacobson, M. (1999), *Fundamentals of Atmospheric Modeling*, 656 pp., Cambridge Univ. Press, Cambridge, U. K.
- Keating, G., J. Y. Nicholson, and L. R. Lake (1980), Venus upper atmosphere structure, *J. Geophys. Res.*, *85*(A13), 7941–7956, doi:10.1029/JA085iA13p07941.
- Keating, G., et al. (1985), Models of Venus neutral upper atmosphere: Structure and composition, *Adv. Space Res.*, *5*(11), 117–171, doi:10.1016/0273-1177(85)90200-5.
- Lellouch, E., J. Goldstein, J. Rosenqvist, S. W. Bougher, and G. Paubert (1994), Global circulation, thermal structure and carbon monoxide distribution in Venus' mesosphere in 1991, *Icarus*, *110*, 315–339, doi:10.1006/icar.1994.1125.
- Mahieux, A., et al. (2008), In-flight performance and calibration of SPICAV/SOIR on-board Venus Express, *Appl. Opt.*, *47*(13), 2252–2265, doi:10.1364/AO.47.002252.
- Mahieux, A., V. Wilquet, R. Drummond, D. Belyaev, A. Fedorova, and A. C. Vandaele (2009), A new method for determining the transfer function of an Acousto optical tunable filter, *Opt. Express*, *17*, 2005–2014, doi:10.1364/OE.17.002005.
- Mahieux, A., A. C. Vandaele, R. Drummond, S. Robert, V. Wilquet, A. Fedorova, and J. L. Bertaux (2010), Densities and temperatures in the Venus mesosphere and lower thermosphere retrieved from SOIR onboard Venus Express. Retrieval technique, *J. Geophys. Res.*, *115*, E12014, doi:10.1029/2010JE003589.
- Mahieux, A., S. Robert, V. Wilquet, R. Drummond, A. C. Vandaele, J. L. Bertaux, and T. S. S. Team (2011), Recent results obtained by the SOIR instrument on board Venus Express: Vertical profiles of carbon species, paper presented at EPSC-DPS Joint Meeting 2011, ASTRIUM, Nantes, France, 4 October.
- Migliorini, A., D. Grassi, L. Montabone, S. Lebonnois, P. Drossart, and G. Piccioni (2012), Investigation of air temperature on the nightside of Venus derived from VIRTIS-H on board Venus-Express, *Icarus*, *217*(2), 640–647, doi:10.1016/j.icarus.2011.07.013.
- Nevejans, D., et al. (2006), Compact high-resolution space-borne echelle grating spectrometer with AOTF based on order sorting for the infrared domain from 2.2 to 4.3 micrometer, *Appl. Opt.*, *45*(21), 5191–5206, doi:10.1364/AO.45.005191.
- Piccilli, A., S. Tellmann, D. Titov, S. S. Limaye, I. V. Khatuntsev, M. Pätzold, and B. Häusler (2012), Dynamical properties of the Venus mesosphere from the radio-occultation experiment VeRa onboard Venus Express, *Icarus*, *217*(2), 669–681, doi:10.1016/j.icarus.2011.07.016.
- Piccioni, G., L. V. Zasova, A. Migliorini, P. Drossart, A. Shakun, A. Garcia Munoz, F. P. Mills, and A. Cardesin-Moinelo (2009), Near-IR oxygen nightglow observed by VIRTIS in the Venus upper atmosphere, *J. Geophys. Res.*, *114*, E00B38, doi:10.1029/2008JE003133.
- Rodgers, C. (1990), Characterization and error analysis of profiles retrieved from remote sounding measurements, *J. Geophys. Res.*, *95*(D5), 5587–5595, doi:10.1029/JD095iD05p05587.
- Rodgers, C. (2000), *Inverse Methods for Atmospheric Sounding: Theory and Practice*, Univ. of Oxford, Oxford, U. K., doi:10.1142/9789812813718.
- Rothman, L. S., et al. (2009), The HITRAN 2008 molecular spectroscopic database, *J. Quant. Spectrosc. Radiat. Transf.*, *110*(9–10), 533–572, doi:10.1016/j.jqsrt.2009.02.013.
- Seiff, A., D. B. Kirk, R. E. Young, R. C. Blanchard, J. T. Findlay, G. M. Kelly, and S. C. Sommer (1980), Measurements of thermal structure and thermal contrasts in the atmosphere of Venus and related dynamical observations: Results from the four Pioneer Venus probes, *J. Geophys. Res.*, *85*(A13), 7903–7933, doi:10.1029/JA085iA13p07903.

- Sonnabend, G., et al. (2012), Thermospheric/mesospheric temperatures on Venus: Results from ground-based high-resolution spectroscopy of CO₂ in 1990/1991 and comparison to results from 2009 and between other techniques, *Icarus*, 217(2), 856–862, doi:10.1016/j.icarus.2011.07.015.
- Taylor, F. W., et al. (1980), Structure and meteorology of the middle atmosphere of Venus: Infrared remote sensing from the Pioneer Orbiter, *J. Geophys. Res.*, 85(A13), 7963–8006, doi:10.1029/JA085iA13p07963.
- Tellmann, S., M. Pätzold, B. Häusler, M. K. Bird, and G. L. Tyler (2009), Structure of the Venus neutral atmosphere as observed by the radio science experiment VeRa on Venus Express, *J. Geophys. Res.*, 114, E00B36, doi:10.1029/2008JE003204.
- Vandaele, A. C., et al. (2008), Composition of the Venus mesosphere measured by SOIR on board Venus Express, *J. Geophys. Res.*, 113, E00B23, doi:10.1029/2008JE003140.
- von Zahn, U., K. H. Fricke, H. J. Hoffmann, and K. Pelka (1979), Venus: Eddy coefficients in the thermosphere and the inferred helium content of the lower atmosphere, *Geophys. Res. Lett.*, 6(5), 337–340, doi:10.1029/GL006i005p00337.
- von Zahn, U., K. H. Fricke, D. M. Hunten, D. Krankowsky, K. Mauersberger, and A. O. Nier (1980), The upper atmosphere of Venus during morning conditions, *J. Geophys. Res.*, 85(A13), 7829–7840, doi:10.1029/JA085iA13p07829.
- Wilquet, V., R. Drummond, A. Mahieux, S. Robert, A. C. Vandaele, and J. L. Bertaux (2012), Optical extinction due to aerosols in the upper haze of Venus: Four years of SOIR/VEX observations from 2006 to 2010, *Icarus*, 217(2), 875–881, doi:10.1016/j.icarus.2011.11.002.
- Zasova, L. V., V. I. Moroz, V. M. Linkin, I. A. Khatuntsev, and B. S. Maiorov (2006), Structure of the Venusian atmosphere from surface up to 100 km, *Cosmic Res. Engl. Transl.*, 44(4), 364–383, doi:10.1134/S0010952506040095.
- Zasova, L. V., N. Ignatiev, I. Khatuntsev, and V. Linkin (2007), Structure of the Venus atmosphere, *Planet. Space Sci.*, 55(12), 1712–1728, doi:10.1016/j.pss.2007.01.011.